Canadian Science Publishing | Canadian Journal of Chemistry

Synthesis of Lanthanide Doped TiO2 Nanoparticles and Their Photocatalytic Activity under Visible Light

Journal:	*Canadian Journal of Chemistry*
Manuscript ID	cjc-2018-0408.R2
Manuscript Type:	Article
Date Submitted by the Author:	05-Mar-2019
Complete List of Authors:	Ndabankulu, Vyolwethu; University of KwaZulu-Natal, School of Chemistry & Physics Maddila, Suresh; University of KwaZulu-Natal, School of Chemistry & Physics Jonnalagadda, Sreekantha Babu; University of KwaZulu-Natal, School of Chemistry & Physics
Is the invited manuscript for consideration in a Special Issue?:	Not applicable (regular submission)
Keyword:	Titanium dioxide, Lanthanides, Visible light, Photocatalytic degrqdation, caffeine

Synthesis of Lanthanide Doped TiO_2 Nanoparticles and Their Photocatalytic Activity under Visible Light

Vuyolwethu O. Ndabankulu, Suresh Maddila and Sreekantha B Jonnalagadda*

School of Chemistry & Physics, University of KwaZulu-Natal, Westville Campus, Chiltern Hills, Durban-4000, South Africa.

***Corresponding Author:** Prof. Sreekantha B. Jonnalagadda

School of Chemistry & Physics,

University of KwaZulu-Natal,

Durban 4000, South Africa.

Tel.: +27 31 2607325,

Fax: +27 31 2603091

E-mail: **jonnalagaddas@ukzn.ac.za**

Abstract:

Four different lanthanide (Ce, Dy, Lu and Sm) doped TiO_2 mesoporous materials were synthesised using sol gel method with titanium (IV) isopropoxide as precursor. All the synthesized materials were characterised using different analytical techniques, BET, PXRD, TEM, SEM-EDX, Raman, FT-IR, Photoluminescence and UV-DRS spectroscopy. Photocatalytic activity and efficacy of the materials in degradation of Caffeine in aqueous solutions was investigated under visible light illumination. While all materials showed good photocatalytic activity, Ce doped TiO_2 exhibited relatively better activity than the other three catalysts. High photo activity of the catalysts was attributed to the presence of lanthanides, and their ability to generate ions that scavenge electrons under visible light, thereby enhancing photo-degradation of Caffeine. All materials proved good and recyclable without loss of catalytic activity up to three runs. An intermediate [*N*-1,3,6-trimethyl-2,4-dioxo-1,2,3,4-tetrahydropyrimidin-5-yl)formamide] (TDTF) and two products (6-amino-1,3-dimethyl-2,4-dioxo-1,2,3,4-tetradropymidin-5-ly)--(methyl)-carbamic acid (ATCA) and *N*-methyl-*N*-(methylcarbomoyl)-2-oxoacetamide (MMO) were identified by the LC-MS spectra.

***Keywords*:** TiO_2, lanthanides, visible light, photo-catalytic degradation, hydroxyl radical, Caffeine.

Introduction:

Pharmaceutical compounds (PC) are a class of emerging contaminates that found widely in the environment.[1,2] PCs have been recurrently detected in wastewater treatment plants (WWTP), surface water and ground water around residential, industrial areas. Reportedly, PCs were noticed in the range from 0.1 to 20 ppb, even in drinking water supplies.[3,4] Due to the high stability and poor biodegradability in water, those substances persist for longer durations in the environment. Pharmaceutical compounds that detected in water systems include non-steroidal anti-inflammatory drugs (NAIDs), endocrine disruptors (EDs)

and stimulants like caffeine.[5] Caffeine is the most used legal stimulant and it is metabolised by humans. It is among the most commonly exploited drugs due to its prevalence in various beverages like coffee, tea and soft drinks. It has good solubility in water. Though, intense utilize of caffeine over time can bring about petulance, transmutation possessions like inhibition of DNA, nervousness and shocks, amongst other side effects. It may stimulate calcium from cells which leads to bone mass loss and is considered as a risk factor for cardiovascular diseases. The presence of caffeine in water produces adverse effects in aquatic organisms, human life and the environment because of its resistance to natural degradation and potential toxicity.[6]

Advanced oxidation processes (AOPs) have found to be one of the powerful methods in removal of organic contaminates in aqueous solution. Photo catalysis using heterogeneous materials is one of the important AOPs applied in the degradation of organic contaminants such as pesticides, dyes, chlorinated aromatics and pharmaceuticals. Recently, photo catalysts received much attention, due to their high stability and extended activity; and scope for easy recovery and reusability. Many AOPs using heterogeneous materials and nanocomposites as photo catalysts using different metal oxides including titania, assisted ultra-violet or visible light (TiO_2/light) have been reported.[7] Photo catalysis is considered effective, because of the use of oxygen as oxidant, plus generation of highly reactive hydroxyl radicals, which facilitate the photodegradation of the organic compounds. Depending on the pH of the solution in most cases super-oxides are also produced, which assist in the process.[8]

Several semi-conductors that exhibit good photocatalytic activity have been reported. Titania (TiO_2) is considered to be one of the best semi-conductors, due to its high stability, good selectivity and environmentally benign properties and cost-effectiveness. Anatase being the most active phase of TiO_2 with wide band gap (E_g = 3.2 eV, anatase) is one of the limitations in its application, because it cannot be used efficiently under visible light, but rather performs better under 5% ultra-violet radiation.[8,9] High carrier charge recombination is also a limiting

factor with using TiO_2 as a photo-catalyst. Doping with metal or non-metal ion is one of the methods used to retard the carrier charge recombination so to increase photo-catalytic efficiency. Oseghe et.al, have reported an efficient method using manganese doped TiO_2 for the photo-catalytic degradation of methyl blue under visible light. Manganese was said to act as an electron trap, there by provoking a red shift allowing the catalyst to absorb light in the visible spectrum.[10] Recently, use of TiO_2 doped with rare-earth metals has received much attention in photocatalytic reactions. Combination of both semiconductors (TiO_2 and Lanthanide) may reduce the charge recombination rate, consuming high utility of light and displaying the absorption in longer wavelengths.[11] Xiao et al. reported a significant red shift, because of doping TiO_2 with samarium, which extended the photocatalytic response into longer wavelength.[12] Previously, we reported the degradation of different pesticides and dyes, using ozone facilitated AOPs and heterogeneous catalysts, including dechlorination of tetrachloro-o-benzoquinone using cesium doped mixed oxides, chloronitrophenol using Ce-V doped mixed metal oxides and photo degradation of 4-chloro-2-methylphenoxyacetic acid using W-doped TiO_2.[13-15]

In this communication, we report the synthesis of four different lanthanide doped TiO_2 materials, their characterization and potential as photo catalysts in degradation of model compound, caffeine under visible light irradiation in aqueous medium.

Experimental Section:

Titanium (IV) isopropoxide (TIP) (MW = 284.22 97 %), non-ionic surfactant (Pluronic F-127), Caffeine (Sigma-Aldrich), Degussa P25 (TiO_2) were supplied by Sigma-Aldrich. Cerium acetylacetonate hydrate, dysprosium oxide, lutetium oxide and samarium acetylacetonate hydrate were of analytical grade and purchased from Sigma-Aldrich. Hydrochloric acid, absolute ethanol and sodium hydroxide were purchased from Promark chemicals in analytical grade.

Catalyst Synthesis

An efficient sol-gel approach was employed for the synthesis of four lanthanide doped (0.5 wt. %) TiO_2. In a typical procedure, 2 g of Pluronic F-127 was dissolved in absolute ethanol (60 ml) under continuous stirring for 4 h. To the resultant clear solution, 6 ml of TIP was added dropwise and stirring was continued for another 2 h. Then, 36 ml of deionised water with lanthanide precursor was added dropwise to the solution. After completion of addition, the solution colour changes from clear to white gel. Further, the stirring of the gel suspension was continued for another 24 h and the resulting mixture was aged overnight in the dark at room temperature. After aging the gel was separated from the solvent by decantation of the solvent. The resulting precipitate was filtered and washed thrice with deionized water and dried at 80-90 °C for overnight. The dried precipitate was calcined at 450 °C for 4 h, in the presence of air, (ramp rate = 2 °C/ min) to obtain the wt.% (0.5) of Ce/Sm/Lu or Dy doped TiO_2 materials.

Product characterisation

Surface morphology of the synthesised material were characterised by use of Scanning electron microscope (ZEISS ULtraplus FEG-SEM). The physical characteristics of the prepared catalyst materials were analyzed using with a transmission electron microscope (JEOL JEM-1010). Bruker D2 phase Powder X-ray diffraction (PXRD) equipped with a Cu – Kα radiation (λ = 0.15401) was used to obtain diffractogram. The texture characterisation was determined using a micrometric flow 3030 instrument. All samples were degassed on micrometric flow prep (060) under nitrogen flow at 90 °C for 1 h. Then temperature was ramped to 200 °C for 12 h to allow the samples to degas before the textural analysis. The Fourier Transmission Infrared (FT-IR) spectrum for the samples was done using a Perkin Elmer Perkin Elmer Precisely 100 FT-IR spectrometer at the 400-4000 cm^{-1} area. Photoluminescence spectra were obtained using (Perkin Elmer LS 55 fluorescence spectrometer) and materials

were excited with high photon energy (310 nm). Raman spectroscopy (532^{TM} bench top spectrometer (Deltanu) was used to identify different phases in the synthesised material. UV-Vis diffuse reflectance spectra were obtained using an Ocean Optic High Resolution Spectrometer (HR 2000+) equipped with a halogen light source (HL – 2000 – FHSA) and an integrating sphere accessory with $BaSO_4$ as a reference.

Hydroxyl radical generation test

An efficient dosimetry approach was employed to identify and quantify the hydroxyl radical formation and concentrations. In a routine run, 100 mg/L of photo catalyst was suspended to a 250 mL of the terephthalic acid (0.1 mM). Then, the solution was irradiated using with a compact fluorescence lamp (26 W/480 Osram Dulux - F378 daylight). All the samples were collected in every 20 min intervals for analysis. The collected sample was centrifuged for 2 min at 14000 r/min and it was further filtered with 0.45 micron before it was analysed using a PerkinElmer LS 55 fluorescence spectrophotometer. Product (2-hydroxyterephthalic acid) formation was identified at 425 nm wavelength using an excitation wavelength of 310 nm.

Photo catalytic Experimental

Photo degradation experiments of caffeine in the laboratory were conducted using CFL as light source. The lamp was fitted into a cylindrical Pyrex jacket to cover the lamp. The reaction vessel was a 1 L Pyrex beaker, which was placed on a magnetic stirrer and lamp in the jacket was fitted in a reaction vessel. 300 mL of caffeine solution was used in each experiment. For optimization experiments, 15, 10, and 5 mg L^{-1} of caffeine was used. In a typical experiment, 50 mg of catalyst was added into caffeine solution and the solution was then sonicated for 10 min and stirred in the dark for 1 h before light illumination. Dark experiment was performed to establish adsorption–desorption equilibrium. Then, the solution was the irradiated with 26 W day light fluorescence lamp for 2 h. Samples were taken at 20 minute

intervals starting from t = 0. Further, 4 mL sample solution was centrifuged using with micro centrifuge (Mikro 120) for 2 min at rpm of 14000. Samples were then analysed using a double beam Shimadzu UV-Vis spectrophotometer. Photo-catalytic degradation observed by monitoring the change in absorbance of caffeine at wavelength 271 nm. In other to identify the intermediates / products of Caffeine degradation, UPLC-ESI–MS analysis in the negative mode was used to obtain the mass spectra with an injection volume of 10 µL. Waters Aquity UPLC with BEH C18 (1.7 mm, 2.1 mm, 100 mm, 35 ^{o}C) column was used. The mobile phase (flow rate 0.15 mL.min^{-1}) was a composed of acetonitrile and water acidified to 0.1% acetic acid (1:1, v/v).

Results and discussion

Transmission electron microscope

HRTEM micrographs at the same magnification are illustrated in **Figure 1**, for all the four materials synthesised (a) Ce-TiO_2, (b) Dy-TiO_2, (c) Lu-TiO_2, and (d) Sm-TiO_2. Continuous lattice was used to confirm the crystalline nature of the as prepared materials. Lattice fringes were observed in all images indicating the anatase crystallographic plane. It was noted that d spacing increases with the ionic radius of the metal ion doped in TiO_2. The HRTEM suggests that the particles were agglomerates and aggregates and then dispersed.

Scanning electron microscope

Figure 2(a) displays SEM micrographs of as prepared materials, (a) Ce-TiO_2, (b) Dy-TiO_2, (c) Lu-TiO_2, and (d) Sm-TiO_2. An observation of the displayed images, suggests that all as prepared materials showed agglomerated irregular shaped particles with inter-particle voids, which is associated with loose particle aggregates. Cerium doped material had reduced particle size compared to the rest, this was attributed to the crystallinity of the material. The EDX analysis results evidently specify the presence of respective lanthanide species on the surface of titania as all dopants (**Figure 2(b)**).

BET N_2 – sorption / desorption studies

N_2 sorption - desorption isotherms were used to determine the textural properties of the lanthanide doped materials and are displayed in **Figure 3**. All the obtained isotherms can be classified as type IV isotherms according to IUPAC with distinct hysteresis loop type III. This was not a surprising, since all materials were mesoporous (2 – 50 nm). Results summarised in table 1 suggest that loaded metal play a crucial role in the surface area and pore volume of the material. Depending on the metal ion used, different values were obtained (**Table 1**). The increase in BET surface area and pore volume may imply enhanced capability for organic pollutant adsorption, which could lead to the improvement of photo-catalytic activity of the as prepared materials.

XRD analysis

Figure 4 shows the XRD diffraction patterns of lanthanide doped titania (0.5%) powder samples calcined at 450 °C. All doped TiO_2 exhibit similar XRD pattern that were all attributed to anatase phase according to (JCPDS file No: 21-1272), 2θ = 25.28° (101), 36.95°, 48.05°, 55.06°, 62.69°, 70.91°. The only difference was with respect to the diffraction peaks; they were slightly shifted relative to one another. There were no additional peaks or phases for lanthanides were detected which means lanthanides are either amorphous or amalgamated into the anatase structure. In addition the dopant concentration was also small to be strikingly noticed by the instrument. The average crystallite size for the anatase diffraction peak (101) was calculated using Debye–Scherrer formula and are shown in table 1

$$D = \frac{K\lambda}{\beta \mathrm{Cos}\theta}$$

Where D is the crystallite size in nm, k is Scherrer's constant ≈ 0.9, λ is the wavelength of the X-ray radiation (Cu$K\alpha$ = 0.15406 nm). β is the corrected band broadening (full width at half-maximum (FWHM)) of the diffraction peak, and θ is the diffraction angle. All the La-

doped materials were polycrystalline in nature and their crystalline sizes are tabulated in table.1.

Raman analysis

Raman spectroscopy was utilised to examine structural changes of the as prepared TiO_2 material. Anatase TiO_2 crystal has six Raman active modes of vibrations and three are IR active. These active bands are found at approximate wave numbers, 146 (E_g), 197 (E_g), 409 (B_{1g}) at 515 (A_{1g}) which is superimposed at 519 (B_{1g}) and 639 cm^{-1} (E_g).[16-19] Not all of the bands are observed in the given figure. All the materials showed the same pattern, with an exception of a band broadening that was observed for cerium doped materials. This observation was attributed to structural changes occurring when Ce ions doped in the lattice structure of TiO_2. No extra band peaks were observed in all the catalyst materials due to low concentrations of dopants which were not detected by the instrument. The crystallinity in the as prepared TiO_2 materials was seen using Raman bands, since Raman lines become weak and broad when the material exhibit local lattice defects.[20] As seen in **Figure 5**, Raman bands of all dopants are broad and have overlapping feature which implies nano-crystals are imperfect. This was also confirmed by powder XRD measurements since it was determined that all the materials are polycrystalline in nature.

FT-IR analysis

Figure 6 shows FTIR of Ce, Dy, Lu and Sm doped TiO_2. TiO_2 with high specific surface area is known to absorb water molecules on the active sites on its surface and form Ti^{4+} - OH_2 on the surface.[21] The presence of physisorbed water molecule is determined by the appearance of absorption band around 1630 cm^{-1},[22] this band appears in all the as prepared materials. A study shows that the water molecule plays an important role in phase transformation of anatase to rutile. The broad band around 3400 cm^{-1} is ascribed to hydroxyl

group.[23] The absorption band around 400 – 800 cm^{-1} is attributed to the anatase TiO_2 skeletal to O – Ti – O and Ti – O bonds. The band at 1400 is due to Ti – O – Ti vibration.[14,24]

UV-DRS analysis

UV-Visible DRS of all the as prepared materials are depicted in **Figure 7**. From the spectrum it can be seen that for all materials the absorption was shifted towards the longer wavelength, i.e. a typical a red shift can be observed. Ceria doped TiO_2 exhibited highest red shift compared with others and Dy had the lowest. The typical red shift is attributed to charge-transfer transition between the electrons of rare earth metal ion and TiO_2 conduction or valence band.[25] Ce has an unpaired electron in its orbital, which creates new filled energy levels with TiO_2, which results in covalent bonding of Ce on the TiO_2 surface and this leads to an enhanced red shift compared to other metal ions.[26]

The optical band gap of the prepared material was calculated from the Tauc plot in fig.6 (b).

$$(\alpha h\nu)^2 = A\,(h\nu - E_g)$$

where hν is the photon energy, α is the absorption coefficient, $\alpha = (\frac{4\pi k}{\lambda})$, k = absorption index/ absorbance, λ = wavelength and A = a constant relative to the material. In broadly, in all prepared materials there was a reduction in band gap and this was attributed to the presence of metal ion in the lattice structure of TiO_2. Dy doped TiO_2 had the lowest band gap reduction with 3.19 eV, followed by Lu with 3.14 eV, Sm^{3+} 3.09 eV and the highest band reduction was that Ce with 3.08 eV. From the obtained results, it can be expected that under visible light cerium doped TiO_2 to be the most effective.

Photoluminescence analysis

Photoluminescence is used in determining the effectiveness of charge transfer, migration, and trapping of charge carriers.[27,28] **Figure 8** displays the PL emission spectra of Ce, Dy, Lu, and Sm doped TiO_2. It is seen that the Dy – TiO_2 had the highest intensity and Ce has the lowest, this suggests that Ce doped TiO_2 will have the highest photo-catalytic

performance. PL emission is caused by the recombination of the excited electron and generated hole; thus low PL means slow rate of recombination. The characteristic peaks of TiO_2 were found between 350 and 540 nm. PL of TiO_2 anatase is attributed to three types of phenomenon, Oxygen vacancies, surface state defects and self-trap excitons.[29-31] Peaks appearing at shorter wave numbers (360 – 380 nm) are attributed to exciton recombination. The decrease in emission intensity was attributed to oxygen vacancy or defects caused by the metal which lead to an increase in optical properties.[21,32,33] The peaks observed at 410 nm at 470 nm are respectively attributed to band-edge free exciton and bound exciton luminesce.[34,35] The dominant peaks between 480 nm and 530 are due to self-trap exciton and oxygen vacancies. An examination of the spectra illustrated in figure 7 shows that there is varied decrease in band gap depending on the metal ion used. Cerium shows the lowest intensity in the PL spectrum with the shortest band gap while dysprosium doped TiO_2 showed the highest intensity with the longest band gap. The results summarised in figure 8 suggests that Ce/TiO_2 will exhibit higher photocatalytic activity compared with other metal ions.

Photo-catalytic experiments

OH radical generation experiment

Aqueous solution of terephthalic acid is the standard chemical used as sensitive chemical dosimetry system in radiation chemistry.[36] Dosimetry analysis was employed to estimate the formation of OH radicals from the as-prepared photo-catalyst. The as prepared materials were illuminated in terephthalic acid solution (0.1 mM) under visible light 28 W (CFL). **Figure 9(a)** displays the PL spectra of 2-hydrxyterephthalic acid obtained, when terephthalic acid was reacted with Ce doped TiO_2 for 120 min. The product formation was followed monitoring the absorbance at 425 nm. While the light intensity was kept constant, the fluorescence intensity was observed to increase over time. Since the resultant spectra are identical in shape to that of 2-hydrxyterephthalic acid, it was assumed that the product formed

as results of Ce doped TiO_2 photo catalysis is caused by the reaction of OH radicals and terephthalic acid (**Scheme 1**). The amount of OH radicals formed by the photo-catalyst is directly dependent on the visible light absorbed by the catalyst. Although, terephthalic acid can directly reacts with photo-generated holes, to give the hydroxyl added product by radical cation, it is known that aromatic compounds are easily oxidised by OH radicals compared with TiO_2 photo-generated hole.[37]

Figure 9(b) shows the relative efficiency of different of as-prepared catalysts, in the formation of 2-hydroxyterephthalic acid with time. The obtained results showing Ce doped material with good efficiency relative to others are in agreement with prediction based on the reduced band gap Ce doped TiO_2 (Fig.7 (b)). This means that charge recombination in Ce-TiO_2 has retarded, compared with other prepared materials.

Photo-catalytic degradation of caffeine

Caffeine is one of the mostly consumed pharmaceutical and it is frequently detected in wastewater. **Figure 10** displays the photo catalytic degradation of caffeine as a function of time in the presence of different lanthanide doped TiO_2 materials used as photo-catalyst under otherwise similar conditions. It is well known that dopants are required to enhance the space charge region potential of TiO_2.[38,39] Charge carrier recombination plays a crucial role in TiO_2 photo-catalysis, the type of metal dopant used is responsible for the process. In lanthanide doped TiO_2, it has been reported that lanthanide-ions could act as electron scavengers which trap electrons from the CB of TiO_2, this is assumed to occur when lanthanide ions are acting as Lewis acids because they are better than O_2 molecule in trapping CB electrons.[40] From the degradation profiles of caffeine illustrated in fig.10, it can be observed that cerium doped TiO_2 exhibits better photo-catalytic activity than all other as prepared materials. These results are in agreement with earlier observations, where Ce/TiO_2 showed a greater red-shift compared to other dopants. Red-shift allows the photo-catalyst to absorb photons in longer wavelength,

thereby increasing the photo-catalytic activity of the catalyst. This leads to formation of more hydroxyl radicals for degradation of caffeine in presence of visible light.

The kinetic data was analysed and the ln [caffeine] versus time plots gave good straight lines, as displayed in fig.11 suggesting the degradation of caffeine follow a pseudo first-order kinetics. The rate constants and R^2 values are shown in **Table 2**. Cerium doped catalyst had the highest rate constant of 3.0 $\times 10^{-3}$ min^{-1}. The photo-generated holes play a vital role in degradation process, when charge separation is preserved, the electron and hole migrate to the photo-catalyst surface where they participate in redox reactions with the adsorbed molecule. The respective rate constants and half-lives for the four photo-catalysts were evaluated (**Figure. 10 and 11**) and results are summarised in Table 2.

Identification of intermediates and products

The intermediates and products were analyzed with Shimadzu, LC-MS TOF mode. Analysis was done over the period of 15 minutes with the retention time between 3 to 4 minutes. Analysis was done by sampling after 20 minutes starting from pure caffeine. From the degradation, one intermediate [*N*-1,3,6-trimethyl-2,4-dioxo-1,2,3,4-tetrahydropyrimidin-5-yl)formamide] (TDTF) and two products (6-amino-1,3-dimethyl-2,4-dioxo-1,2,3,4-tetradropymidin-5-ly)(methyl)carbamic acid (ATCA) and *N*-methyl-*N*-(methylcarbomoyl)-2-oxoacetamide (MMO) were identified (**Scheme 2**) after 120 minutes of irradiation and they eluted in the retention time 3.47 minutes. All the identified products are shown in the supporting information (**S1**).

A possible reaction mechanism for the formation of various products could be assumed in terms of the ways concerning electron transfer reactions and reaction with hydroxyl radicals ($OH^{\cdot}$) is revealed in Schemes 2 respectively. Caffeine on attack by a hydroxyl radical can lead to the formation of an intermediate radical species, which undergoes cyclic ring dissection, generating the main intermediate (TDTF) product observed during the photo catalyzed

degradation. Then this species can add an oxygen atom to form ATCA. ATCA on further transfer of an electron, lose the amide group to form a stable product, MMO.

Conclusion

Four lanthanides, Ce, Dy, Lu and Sm doped TiO_2 mesoporous materials were synthesised and characterised by using different techniques. XRD pattern showed that all the as prepared materials were polycrystalline in nature. All the as prepared materials showed a red shift, towards longer wavelength and their photo activity was assessed under visible light. Hydroxyl radicals have been generated from each of the as prepared materials during the reaction. Ce doped TiO_2 showed better activity than rest of the catalysts. The observed high photo activity of the catalysts was attributed to the ability of lanthanides to generate ions which can scavenge electrons, thereby enhancing photo degradation of caffeine under visible light.

Acknowledgement

The authors are thankful to the National Research Foundation (NRF) of South Africa, and University of KwaZulu-Natal, Durban, for financial support and research facilities.

References

[1] Maddila, S.; Jonnalagadda, S.B. Pharmaceu. Chem. J., **2013**, 46, 1-6.

[2] Maddila, S.; Jonnalagadda, S.B. Arch. Der Pharm. Life Sci., **2012,** 345, 163-168

[1] He, Y.; Sutton, N.B.; Rijnaarts, H.H.H.; Langenhoff, A.A.M. Appl. Catal. B: Environ., **2016**, 182, 132–141.

[2] Kasprzyk-Hordern, B.; Dinsdale, R.M.; Guwy, A.J. Environ. Poll., **2009**, 157, 1773–1777.

[3] Trovo, A.G.; Silva, T.F.S.; Gomes Jr, O.; Machado, A.E.M.; Neto, W.B.; Muller Jr, P.S.; Daniel, D. Chemosphere, **2013**, 90, 170–175.

[4] Rosal, R.; Rodriguez, A.; Perdigón-Melon, J.A.; Petre, A.; Garcia-Calvo, E.; Gomez, M.J.; Aguera, A.; Fernandez-Alba, A.R. Chemosphere, **2009**, 74, 825–831.

[5] Broseus, R.; Vincent, S.; Aboulfadl, K.; Daneshvar, A.; Sauve, S.; Barbeau, B.; Prevost, M. Water Res., **2009**, 43, 4707–4717.

[6] Rong, C.; Hongyu, J.; Yu-You, L. Chem. Eng. J., **2018**, 334, 444–452.

[7] Zarubica, A.; Vasic, M.; Antonijevic, M.D.; Randelovic, M.; Momcilovic, M.; Krstic, J.; Nedeljkovic, J. Materials Res. Bull., **2014**, 57, 146–151.

[8] Zhang, Z.; Wang, X.; Long, J.; Gu, Q.; Ding, Z.; Fu, X. J. Catal., **2010**, 276, 201–214.

[9] Naraginti, S.; Thejaswini, T.V.L.; Prabhakaran, D.; Sivakumar, A.; Satyanarayana, V.S.V.; Arun Prasad, A.S. Spectrochim. Acta, Part A, **2015**, 149, 571–579.

[10] Oseghe, E.O.; Ndungu, P.G.; Jonnalagadda, S.B. Environ. Sci. Poll. Res., **2015**, 22, 211–222.

[11] Reszczynska, J.; Grzyb, T.; Sobczak, J.W.; Lisowski, W.; Gazda, M.; Ohtani, B.; Zaleska, A. Appl. Catal. B: Environ., **2015**, 163, 40–49.

[12] Xiao, Q.; Si, Z.; Yu, Z.; Qiu, G. Mater. Sci. Eng., B, **2007**, 137, 189–194.

[13] Maddila, S.; Dasireddy, V.D.B.C.; Jonnalagadda, S.B. Appl. Catal. B: Environ., **2014**, 150–151, 305–314.

[14] Oseghe, E.O.; Ndungu, P.G.; Jonnalagadda, S.B. J. Photochem. & Photobiol. A: Chem., **2015**, 312, 96–106.

[15] Maddila, S.; Dasireddy, V.D.B.C.; Jonnalagadda, S.B. Appl. Catal. B: Environ., **2013**, 138–139, 149–160.

[16] Kelly, S.; Pollak, F.H.; Tomkiewicz, M. The J. Phy. Chem. B, **1997**, 101, 2730–2734.

[17] Gajovic, A.; Stubicar, M.; Ivanda, M.; Furic, K. J. Mol. Stru., **2001**, 563–564, 315–320.

[18] Jabbari, V.; Hamadanian, M.; Shamshiri, M.; Villagran, D. RSC Advan., **2016**, 6, 15678–15685.

[19] Xiang, C.; Li, M.; Zhi, M.; Manivannan, A.; Wu, N. J. Mater. Chem., **2012**, 22, 19161–19167.

[20] Choudhury, B.; Choudhury, A. Internat. Nano Lett., **2013**, 3, 1–9.

[21] Tripathi, A.K.; Singh, M.K.; Mathpal, M.C.; Mishra, S.K.; Agarwal, A. J. Alloys and Compounds, **2013**, 549, 114–120.

[22] Zhao, Y.; Li, C.; Liu, X.; Gu, F.; Jiang, H.; Shao, W.; Zhang, L.; He, Y. Mater. Lett., **2007**, 61, 79–83.

[23] Park, J.T.; Koh, J.H.; Seo, J.A.; Kim, J.H. J. Mater. Chem., **2011**, 21, 17872–17880.

[24] Dias, C.F.B.; Araujo-Chaves, J.C.; Mugnol, K.C.U.; Trindade, F.J.; Alves, O.L.; Caires, A.C.F.; Brochsztain, S.; Crespilho, F.N.; Matos, J.R.; Nascimento, O.R.; Nantes, I.L. RSC Advan., **2012**, 2, 7417–7426.

[25] Yan, N.; Zhu, Z.; Zhang, J.; Zhao, Z.; Liu, Q. Mater. Res. Bull., **2012**, 47, 1869–1873.

[26] Shi, Z.-L.; Du, C.; Yao, S-H. J. Taiwan Institute of Chem. Eng., **2011**, 42, 652–657.

[27] Wang, X.; Feng, Z.; Shi, J.; Jia, G.; Shen, S.; Zhou, J.; Li, C. Phy. Chem. Chem. Physic., **2010**, 12, 7083–7090.

[28] Yan, J.; Wu, G.; Guan, N.; Li, L.; Li, Z.; Cao, X. Phy. Chem. Chem. Physic., **2013**, 15, 10978–10988.

[29] Khan, M.M.; Ansari, S.A.; Pradhan, D.; Ansari, M.O.; Han, D.H.; Lee, J.; Cho, M.H. J. Mater. Chem. A, **2014**, 2, 637–644.

[30] Roy, J.S.; Pal Majumder, T.; Dabrowski, R. J. Mol. Struct., **2015**, 1098, 351–354.

[31] Rajabi, M.; Shogh, S.; Iraji zad, A. J. Lumines., **2015**, 157, 235–242.

[32] Oseghe, E.O.; Ndungu, P.G.; Jonnalagadda, S.B. Environ. Sci. & Poll. Res., **2015**, 22, 211–222.

[33] Kernazhitsky, L.; Shymanovska, V.; Gavrilko, T.; Naumov, V.; Fedorenko, L.; Kshnyakin, V.; Baran, J. J. Luminesc., **2015**, 166, 253–258.

[34] Hu, L.; Song, H.; Pan, G.; Yan, B.; Qin, R.; Dai, Q.; Fan, L.; Li, S.; Bai, X. J. Luminesc., **2007**, 127, 371–376.

[35] Nakajima, H.; Mori, T.; Shen, Q.; Toyoda, T. Chem. Phy. Lett., **2005**, 409, 81–84.

[36] Barreto, J.C.; Smith, G.S.; Strobel, N.H.P.; McQuillin, P.A.; Miller, T.A. Life Sci., **1994**, 56, PL89–PL96.

[37] Myilsamy, M.; Mahalakshmi, M.; Murugesan, V.; Subha, N. Appl. Surface Sci., **2015**, 342, 1–10.

[38] Li, F.B.; Li, X.Z.; Hou, M.F.; Cheah, K.W.; Choy, W.C.H. Appl. Catal. A: Gen., **2005**, 285, 181–189.

[39] Karakitsou, K.E.; Verykios, X.E. The J. Phy. Chem., **1993**, 97, 1184–1189.

[40] Silva, A.M.T.; Silva, C.G.; Drazic, G.; Faria, J.L. Catal. Today., **2009**, 144, 13–18.

Captions: Figures and schemes

Figure 1: HRTEM micrographs of (0.5 wt%) (a) Ce (b) Dy (c) Lu and (d) Sm doped TiO_2 prepared materials

Figure 2(a): SEM micrographs of (0.5 wt%) (a) Ce (b) Dy (c) Lu and (d) Sm doped TiO_2 as prepared material

Figure 2 (b). EDX spectrum of lanthanide doped TiO_2.

Figure 3: N_2 sorption and desorption isotherms of 0.5 wt%) (a) Ce (b) Dy (c) Lu and (d) Sm doped TiO_2 as prepared material

Figure 4: X-ray diffraction of the as prepared material

Figure 5: Raman spectra of Lanthanide doped TiO_2

Figure 6: IR spectra of Lanthanide doped TiO_2 materials

Figure 7: UV-Visible diffuse reflectance (a) and Tauc plot of the as prepared materials (b)

Figure 8: Photoluminescence of Lanthanide doped titania materials

Figure 9: Photoluminescence for the formation of 2-hydroxyterephthalic acid generated by Ce doped TiO_2 in 120 minutes (a) and comparison of product formation using different catalyst (b) OH radical generation by 100 mg/L of catalysts in 200 mL 0.1 mM terephthalic acid solution irradiated with 28 W daylight CFL.

Figure 10: Photocatalytic degradation curves of caffeine over 120 min of irradiation with visible light.

Figure 11: First order degradation of caffeine curves

Scheme 1: Formation of 2-hydroxyterephthalic acid

Scheme 2: Possible reaction mechanism

Table 1: Summary of the textural characterizations, XRD and Band gap analysis on the various as- prepared materials

Table.2: Degradation kinetics of caffeine

Tables

Table 1: Summary of the textural characterizations, XRD and Band gap analysis on the various as- prepared materials

Sample	BET Surface area/ m^2g^{-1}	BJH adsorption pore volume/ cm^3g^{-1}	BJH adsorption pore size/ nm	FWHM (101) / rad	Anatase crystal size (101) / nm	Band gap energy/ eV
Ce-0.5 wt.	57.884	0.2229	12.613	0.01902	7.29	3.08
Dy-0.5 wt.	45.6867	0.200033	15.968	0.01779	7.79	3.19
Lu-0.5 wt.	43.5612	0.184053	15.5648	0.01483	9.35	3.14
Sm-0.5 wt.	45.5546	0.165380	13.888	0.01763	7.86	3.09

Table.2: Degradation kinetics of caffeine

Sample	Rate constant (k) / min × 10^{-3}	Half-life / min	R^2
Ce-TiO_2	3.00	231.05	0.9896
Dy-TiO_2	0.80	866.43	0.9244
Lu-TiO_2	1.70	407.73	0.9412
Sm-TiO_2	0.80	866.43	0.9804

Figures and Schemes

Figure 1: HRTEM micrographs of (0.5 wt%) (a) Ce (b) Dy (c) Lu and (d) Sm doped TiO_2 prepared materials

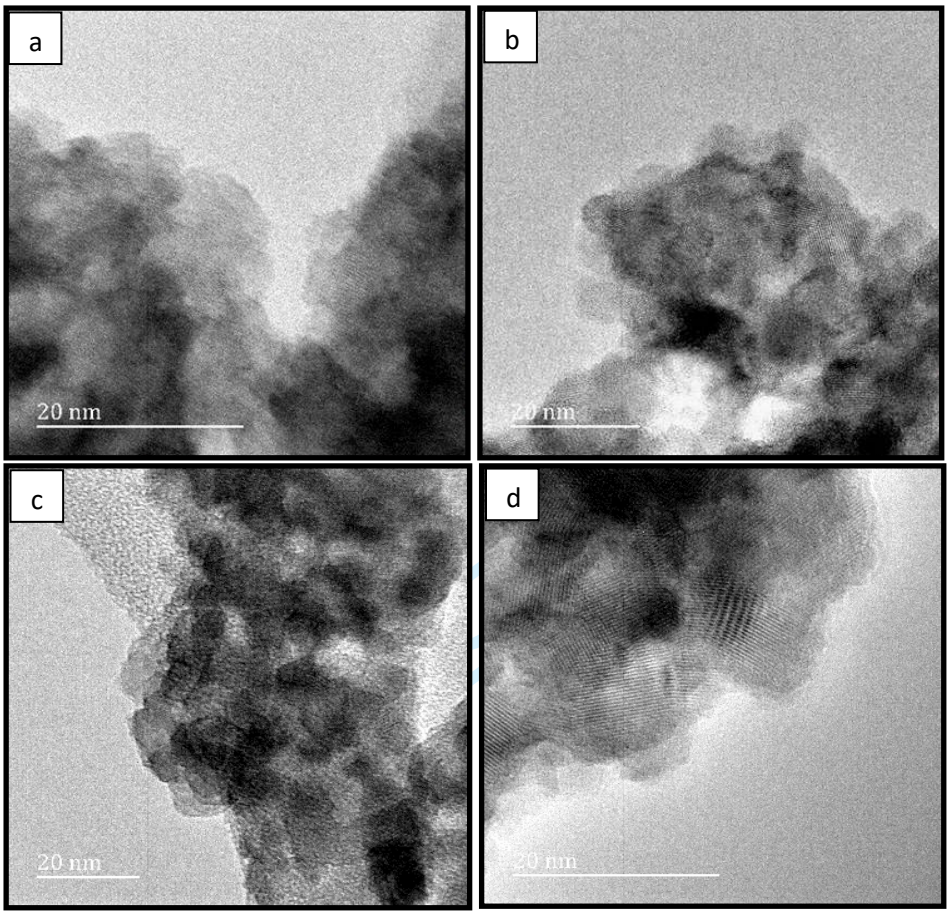

Figure 2(a): SEM micrographs of (0.5 wt%) (a) Ce (b) Dy (c) Lu and (d) Sm doped TiO_2 as prepared material

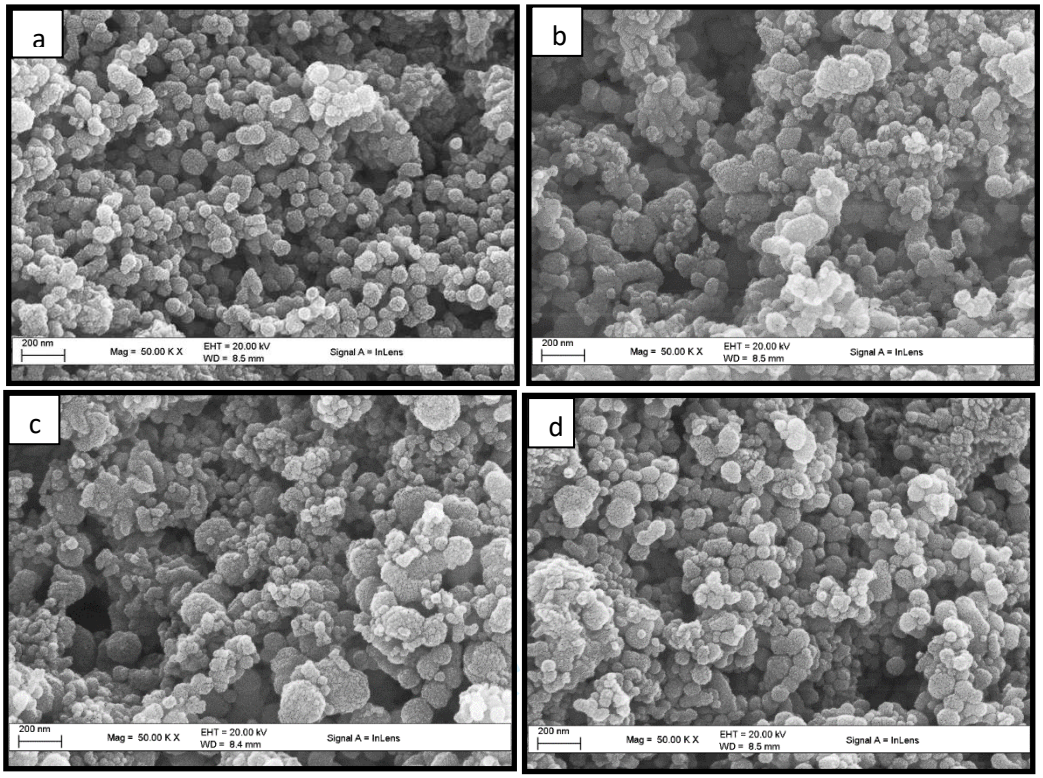

Figure 2 (b). EDX spectrum of lanthanide doped TiO_2.

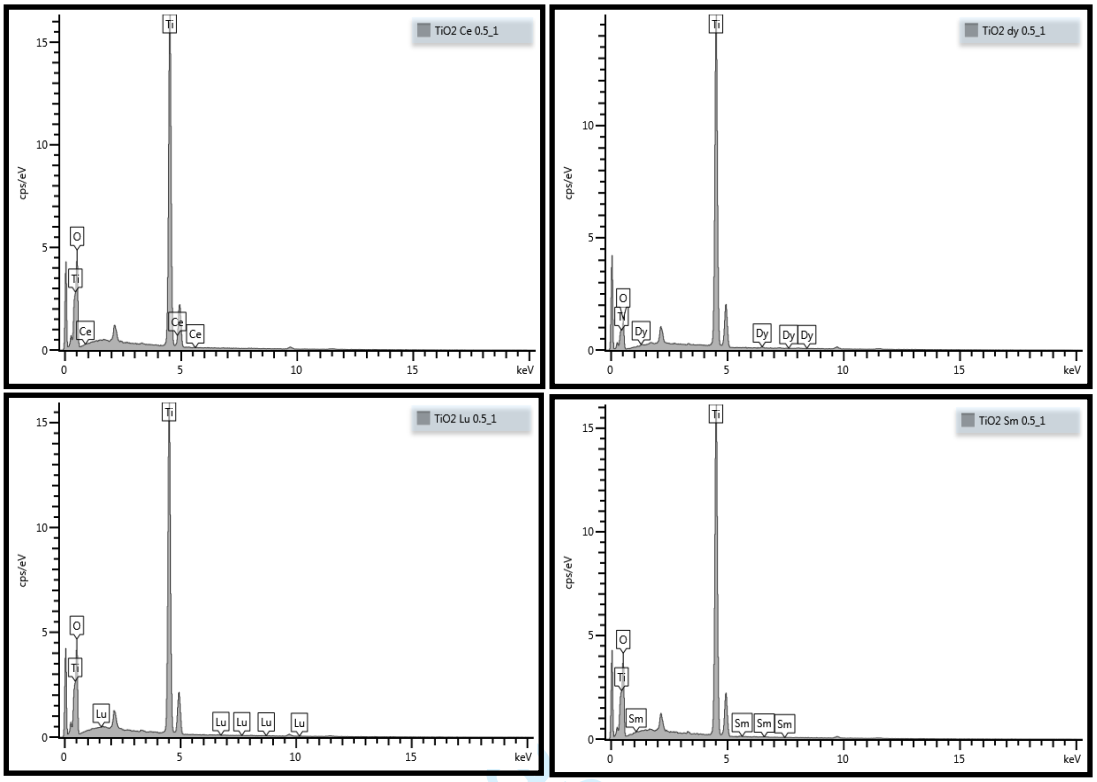

Figure 3: N_2 sorption and desorption isotherms of 0.5 wt%) (a) Ce (b) Dy (c) Lu and (d) Sm doped TiO_2 as prepared material

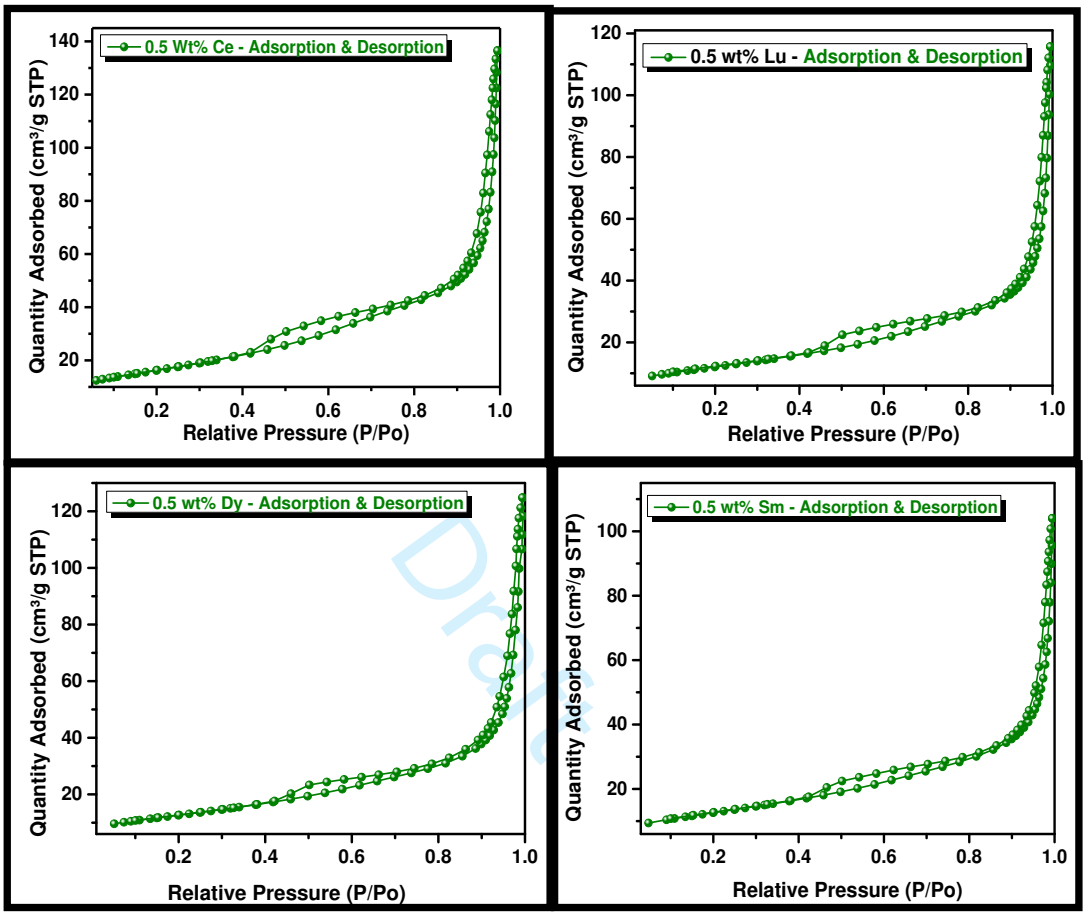

Figure 4: X-ray diffraction of the as prepared material

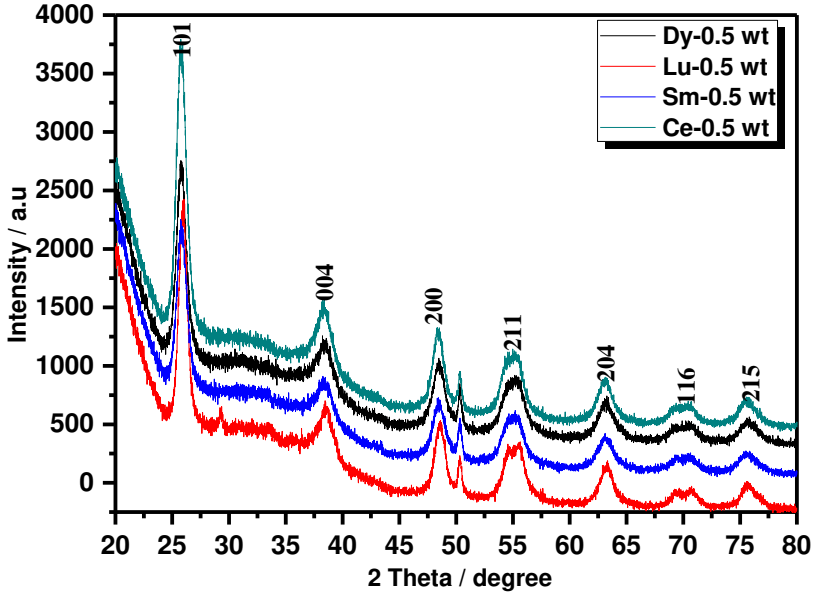

Figure 5: Raman spectra of Lanthanide doped TiO_2

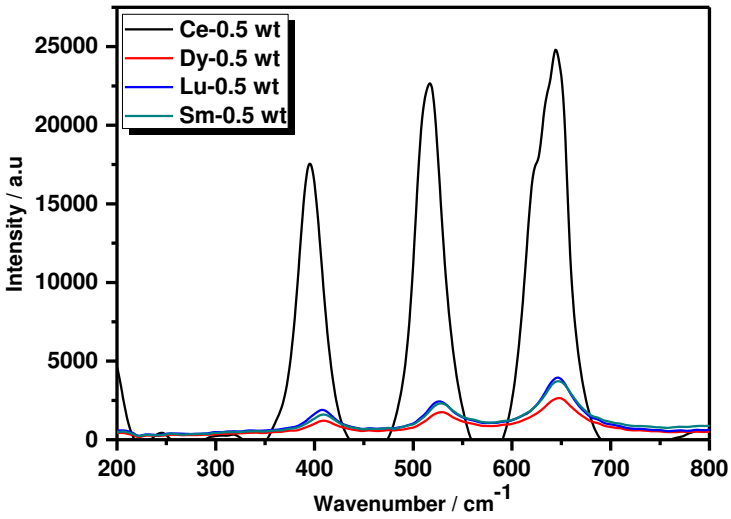

Figure 6: IR spectra of Lanthanide doped TiO_2 materials

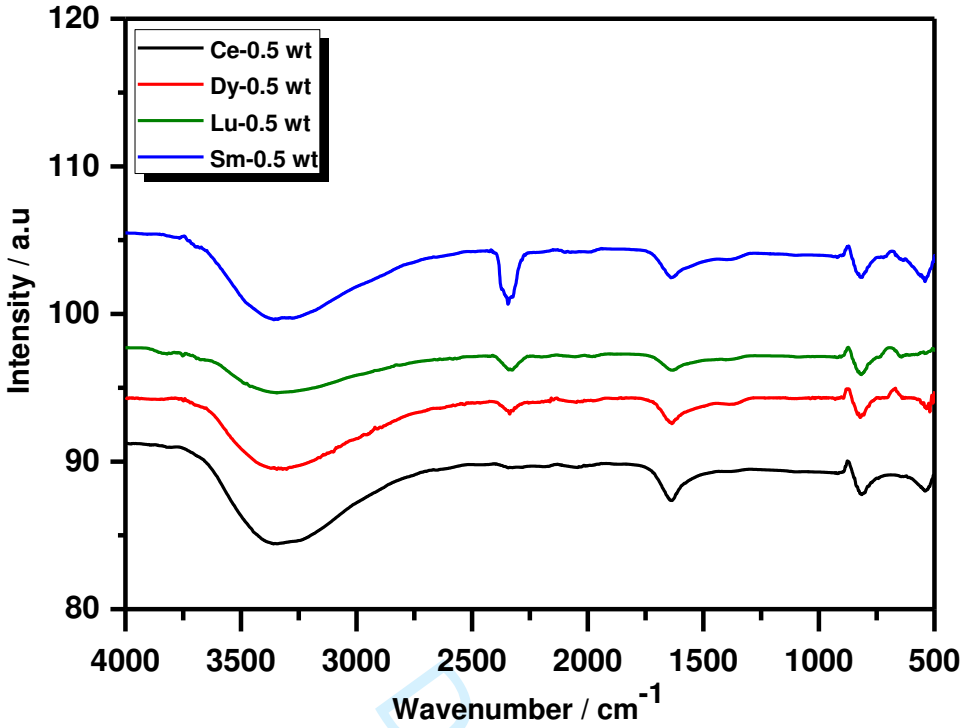

Figure 7: UV-Visible diffuse reflectance (a) and Tauc plot of the as prepared materials (b)

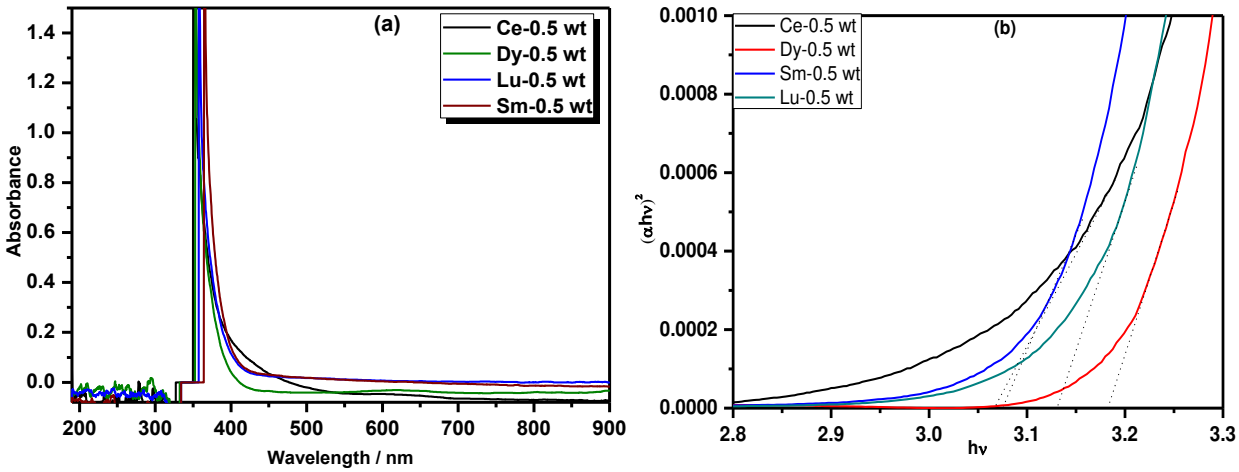

Figure 8: Photoluminescence of Lanthanide doped titania materials

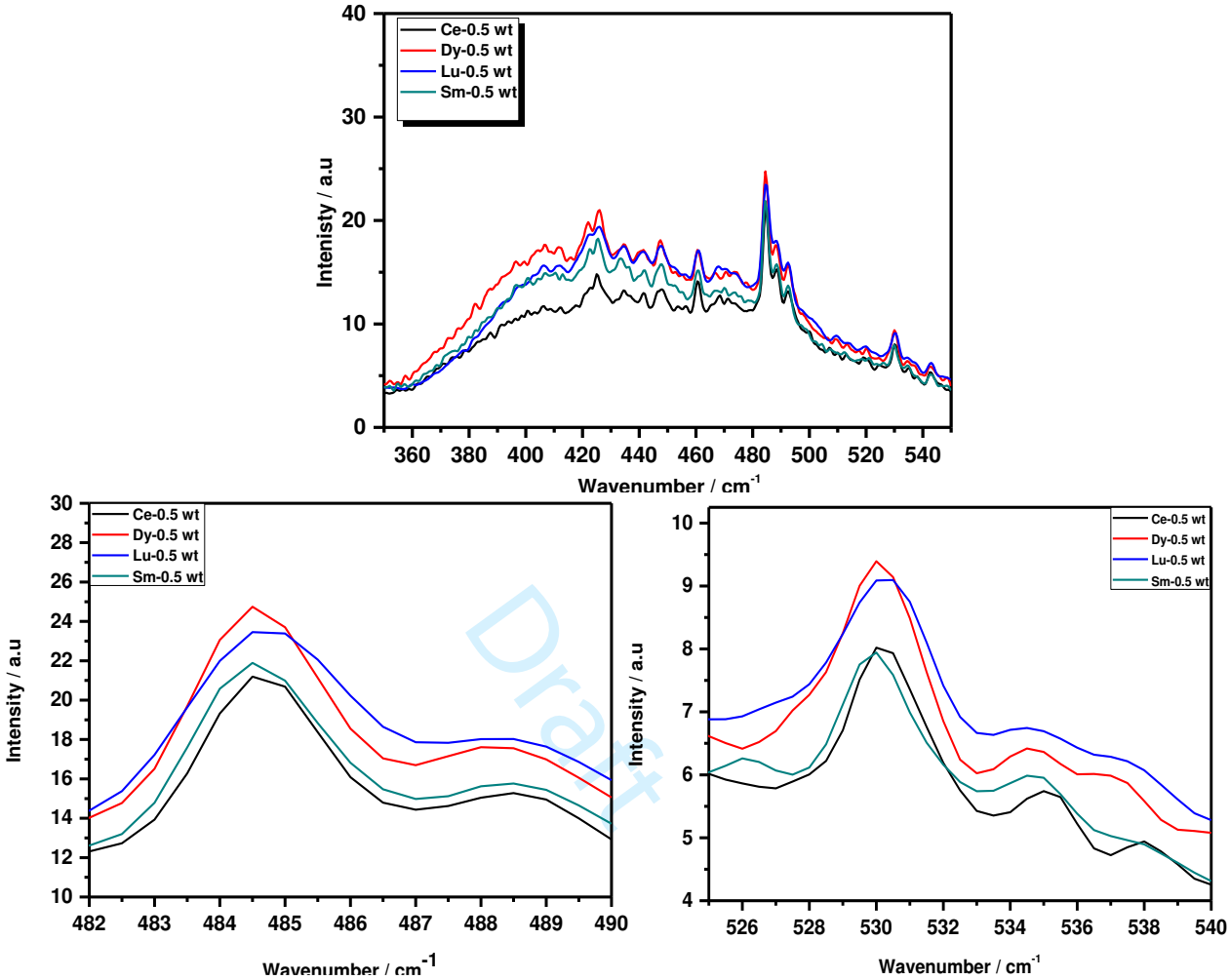

Figure 9: Photoluminescence for the formation of 2-hydroxyterephthalic acid generated by Ce doped TiO_2 in 120 minutes (a) and comparison of product formation using different catalyst (b) OH radical generation by 100 mg/L of catalysts in 200 mL 0.1 mM terephthalic acid solution irradiated with 28 W daylight CFL.

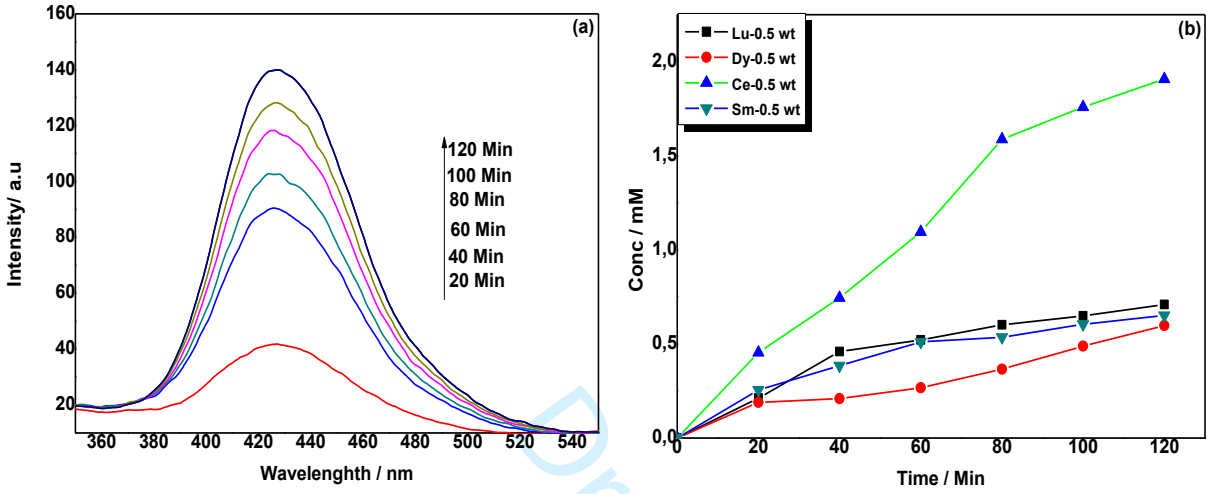

Figure 10: Photocatalytic degradation curves of caffeine over 120 min of irradiation with visible light

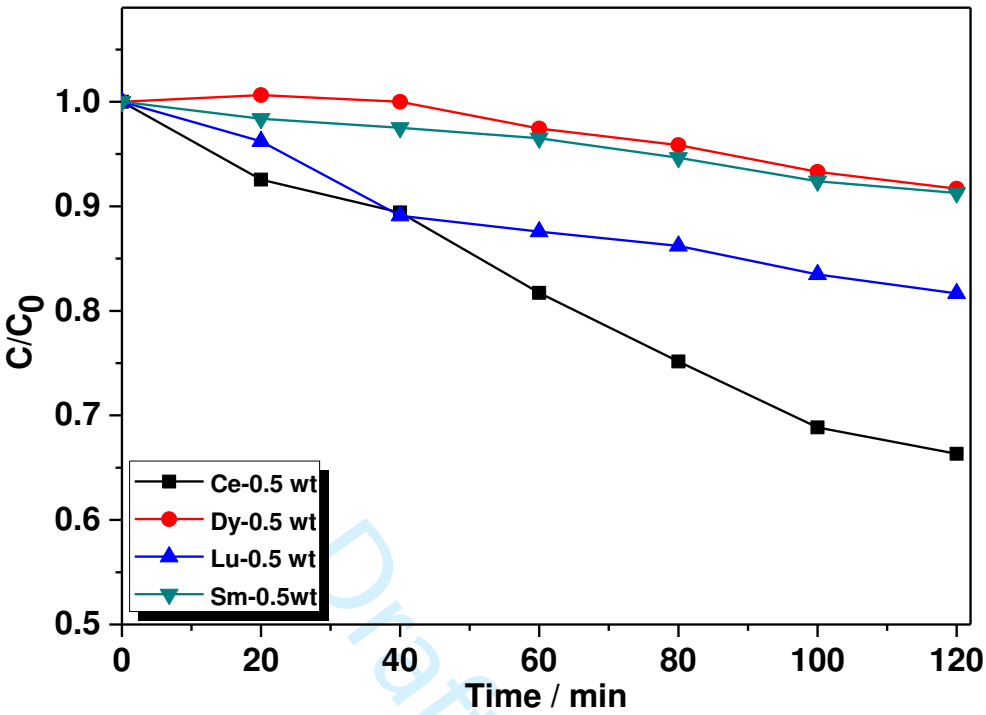

Figure 11: First order degradation of caffeine curves

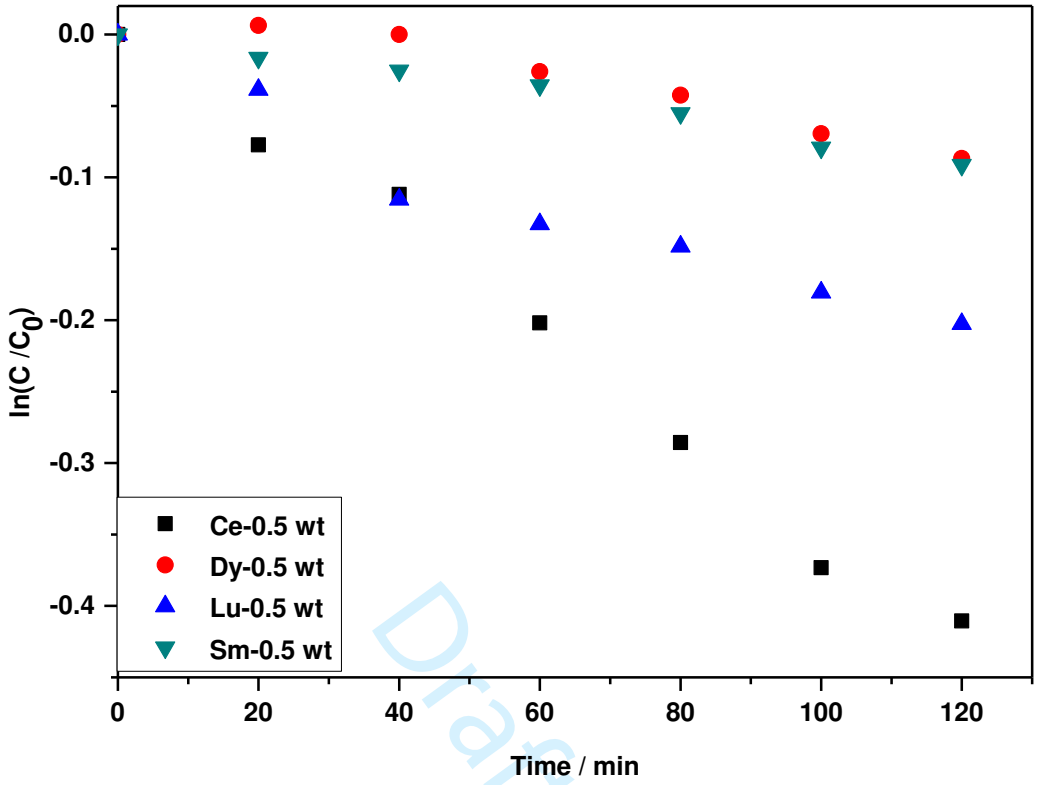

Scheme 1: Formation of 2-hydroxyterephthalic acid

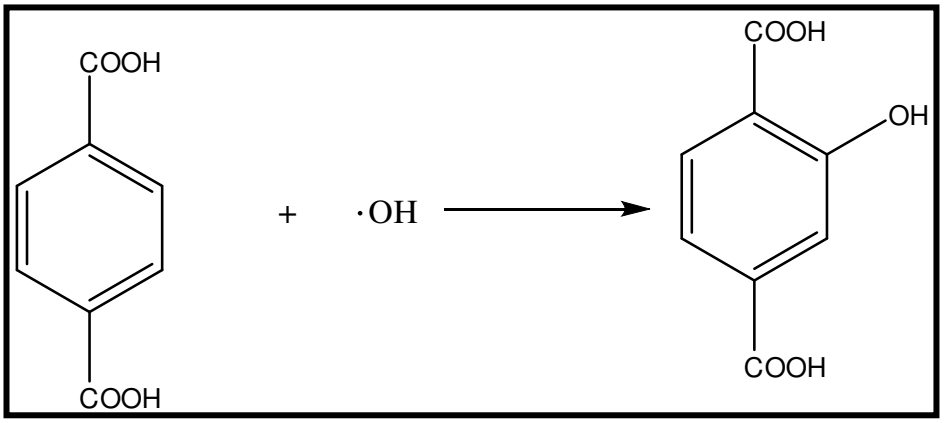

Scheme 2: Possible reaction mechanism